Efficient Improvement of Photovoltaic-Battery Systems in Standalone DC Microgrids Using A Local Hierarchical Control for the Battery System

Yun Yang, *Member, IEEE*, Yaxiao Qin, Siew-Chong Tan, *Senior Member, IEEE* and Ron Hui, *Fellow, IEEE*

***Abstract*--Conventional control methods for the battery systems of photovoltaic (PV)-battery systems in standalone DC microgrids are designed to stringently regulate the bus voltages at the maximum power points (MPP) of PV modules while the state-of-charge (SOC) of the battery packs are regulated within the tolerances. In this paper, a local hierarchical control (LHC) is proposed for the battery system to improve the energy efficiency of the entire PV-battery system at the MPP of PV modules while the SOC of the battery pack is still regulated within the tolerance. Specifically, by allowing the DC bus voltage to deviate within a preset allowable tolerance, the secondary control of the LHC is employed to compute real-time optimal references to its primary control, such that the energy conversion of the entire PV-battery system can be optimized. Simulation studies exhibit significant efficiency improvement of a 12-PV-battery system under both uniform and nonuniform insolation conditions in a cloudy day and a 600-kW PV-battery system in a sunny day using the proposed LHC. Experimental results validate that the energy efficiency of a one-PV-module-battery system controlled by the LHC can be enhanced using shortened sunny-day and cloudy-day irradiance profiles for various PV modules. The proposed control scheme can be easily implemented in digital controllers without additional hardware costs.**

***Index Terms*-- Photovoltaic (PV)-battery system, standalone DC microgrid, local hierarchical control (LHC).**

I. Introduction

PHOTOVOLTAIC (PV) systems have been widely adopted as major power sources of standalone power systems, such as that used in rural power grids, parking meters, trash compactors, charging stations and space-crafts [1]. PV systems adopted together with emerging standalone DC microgrids, such as those used in solar home projects in Africa (e.g. Kenya) [2], have been found to be a convenient and practical means of providing high-quality power to remote areas that were previously inaccessible to cheap and reliable electricity supply. A typical PV system in a standalone DC microgrid comprise multiple decentralized sets of PV modules, their corresponding grid-connected converters, and a battery system. Most ongoing research works on such PV-battery systems are focused on the design of grid-connected converters [3]−[7] and their local control algorithms for achieving maximum-power-point tracking (MPPT), fast dynamic response, stability [7]−[11], and the power flow management of microgrids [12]−[19]. They mainly cover the improvement of the PV-battery systems in various aspects, such as power quality improvement, ensuring grid stability, and simplifying practical implementation. Nevertheless, there remains a research gap concerning the efficiency improvement of the entire PV-battery system that are achievable through the shifting of operating points, and their correlated design, which has not been reported in [20]−[35].

In existing PV-battery systems, either field MPPT (FMPPT) or distributed MPPT (DMPPT) approaches are adopted to control the grid-connected converters to track the MPP of PV modules in both the uniform insolation condition and the nonuniform insolation conditions of clouds, dirtiness, shadows, aging, and manufacturing tolerance [3]−[19], [36]. The MPPT controllers, comprising both FMPPT and DMPPT, can be perturb-and-observation (P&O) control, the incremental-conductance (INC) control, the particle-swarm-optimization (PSO) control, the ripple-correlation control (RCC), the chaos search control, the neural-network control, the fuzzy logic control, and the advanced PSO control [36], etc. They are all designed to achieve maximum extraction of electrical power from the PV modules via the regulations of the input power of the grid-connected converters. As a result, an associated battery system must be utilized to store excess and provide shortfall power in the generation by regulating the DC bus voltage. The battery system is typically controlled by a multi-loop strategy considering the bus voltage and the state-of-charge (SOC) constraints. Specifically, two control loops monitor the SOC of the battery pack to avoid overcharge by regulating the PV operating point less than the MPP and overdischarge by shedding the non-critical loads, respectively. Another control loop ensures the system power balance by regulating the DC bus voltage to the nominal value [37]−[45].

Nevertheless, none of these methods considers the efficiency of the entire PV-battery system as a control variable. Hence, a two-layer local hierarchical control (LHC), comprising the existing battery control as the primary control, is proposed. The objective of the LHC is to improve the efficiency of the entire PV-battery system by fully considering power losses of the PV module, the grid-connected converter and the battery system, while still achieving the MPPT, bus voltage regulation, and the SOC of the battery pack within allowable tolerances. As practical loads (voltage-sensitive loads are equipped with load-side converters) can usually tolerate a certain percentage

Manuscript received November 3, 2018; revised January 9, 2019; accepted February 13, 2019. This work is supported by the Hong Kong Research Grant Council under Theme-based Research Project: T23-701/14-N.

Y. Yang, Y. Qin, and S. C. Tan are with the Department of Electrical and Electronic Engineering, The University of Hong Kong, Hong Kong, China (e-mail: cacaloto@hku.hk, qinyaxiao@gmail.com, sctan@eee.hku.hk).

S. Y. R. Hui is with the Department of Electrical and Electronic Engineering, The University of Hong Kong, Hong Kong, China and also with the Department of Electrical and Electronic Engineering, Imperial College London, London SW7 2AZ, U.K. (e-mail: ronhui@eee.hku.hk).

of voltage offset (conservatively ±5%), the secondary control of the LHC can be designed to search out optimal bus voltages within a preset tolerance as references for the primary control of the LHC. In other words, the relaxation of bus voltage regulation makes the efficiency of the entire PV-battery system optimizable. The major contribution of this paper is to provide a strategy to optimize the efficiency of an entire PV-battery system in a standalone DC microgrid for the first time. This brings benefits of efficiency improvement of PV-battery systems under variable operating conditions, as compared to the conventional methods. For ease of realization, the adopted LHC employs simple equations for the secondary control, working along with the existing battery control as the primary control, which can be easily implemented in digital controllers without any communication. It is important to note that the main contribution of this paper is oriented to a more efficient use of the primary energy source (PV-battery system) without additional hardware costs.

II. Comparisons Between the Conventional Battery Control and the Proposed LHC

A typical PV-battery system in a standalone DC microgrid is depicted in Fig. 1. Here, the PV boost converter is utilized to track the MPP of the PV modules. The battery system, comprising battery packs, a battery management system (BMS), and a bi-directional DC/DC converter, is installed to stabilize the DC bus voltage v_{dc}. The BMS monitors SOC, state-of-health (SOH) and power sharing conditions of the battery pack by measuring the battery current i_B and the battery voltage v_B.

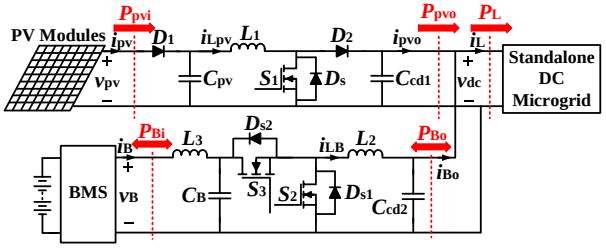

Fig. 1. A typical PV-battery system in a standalone DC microgrid.

The control block diagram of the conventional control method for the PV-battery system in a standalone DC microgrid is shown in Fig. 2. Here, C_{bat} is the nominal capacity of the battery pack. η_{bat} is the charging and discharging coefficient, which is dependent on the aging effect, charging and discharging rate, and temperature of the battery. In the normal operating mode, as the SOC of the battery pack are within the tolerances of the maximum SOC (SOC_{max}) and the minimum SOC (SOC_{min}), the SOC control loops remain idle and the PV modules reference voltage v_{pvref} is only determined by the MPPT controller. The battery pack is charged in the constant current mode via the control of the bi-directional DC/DC converter. Consequently, the PV boost converter injects the maximum power into the DC microgrid by controlling v_{pv} at v_{pvref}. The battery system balances the supplied and the consumed power in the DC microgrid by controlling the DC bus voltage v_{dc} at the nominal v_{dcref}. However, when the SOC of the battery pack reaches SOC_{max}, which means the battery system cannot absorb excess power from the PV modules, the error between the SOC_{max} and the SOC(t), correspondingly, the PI_{B-1} output starts to turn negative. Then, $v_{pvref} > v_{MPPT}$, indicates that the PV operating point moves away from the MPP ($P_{pvi} < P_{MPPT}$). Consequently, the supplied power by the power modules P_{pvi} may be less than the power consumed by the loads in the DC microgrid, which induces a bus voltage drop. To ensure the bus voltage within the tolerance, the battery pack discharges to compensate the insufficient power. The control loop will keep reducing the power extracted from the PV modules until the SOC of the battery pack settles at SOC_{max}. Nevertheless, in case that the SOC is greater than SOC_{max}, the battery management system (BMS) will regulate the battery charging in constant voltage mode to protect the battery pack. Meanwhile, the battery controller stringently regulates the DC bus voltage v_{dc} at the nominal v_{dcref}. Besides, when the SOC of the battery pack reaches SOC_{min}, which means the battery system cannot provide shortage power for the loads, both switches S_2 and S_3 of the bi-directional DC/DC converter of the battery system are turned off by the PV power controller. The reserve diesel generates power to the microgrid to ensure that the DC bus voltage can be regulated by the battery controller to achieve the power balance.

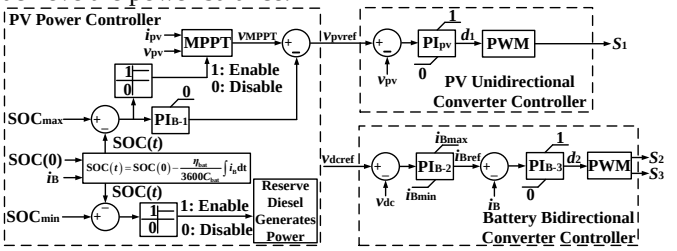

Fig. 2. Control block diagram of the conventional control method for the PV-battery system in a standalone DC microgrid.

The energy efficiency of the entire PV-battery system is

$$\eta_{\text{PV-bat}} = \frac{\int \left(P_{\text{pvi}} - P_{\text{loss}} \right) dt}{\int P_{\text{pvi}} dt}, \tag{1}$$

where P_{loss} is the total power losses of the PV-battery system. When the battery pack absorbs excess power,

$$P_{\text{loss}} = P_{\text{pvi}} - P_{\text{pvo}} + P_{\text{Bo}} - P_{\text{Bi}} \tag{2}$$

and

$$P_{\text{pvo}} = P_{\text{L}} + P_{\text{Bo}} . \tag{3}$$

When the battery pack provides shortage power,

$$P_{\text{loss}} = P_{\text{pvi}} - P_{\text{pvo}} + P_{\text{Bi}} - P_{\text{Bo}} \tag{4}$$

and

$$P_{\text{L}} = P_{\text{pvo}} + P_{\text{Bo}} . \tag{5}$$

Substitute (2), (3) and (4), (5) into (1) respectively, the energy efficiency of the entire PV-battery system can be uniformly expressed as

$$\eta_{\text{PV-bat}} = \frac{\int \left(P_{\text{L}} + P_{\text{Bi}} \right) dt}{\int P_{\text{pvi}} dt} = \frac{\int P_{\text{out}} dt}{\int P_{\text{pvi}} dt}, \tag{6}$$

where $P_{Bi} > 0$ indicates that the battery pack absorbs excess power; $P_{Bi} < 0$ indicates that the battery pack provides shortage power; P_{out} is the total output power.

Obviously, the energy efficiency of the entire PV-battery system is not considered in the conventional control designs. To extend the control objective by incorporating $\eta_{PV\text{-}bat}$ as a control variable, a two-layer local hierarchical control (LHC) is

proposed. The control block diagram of the LHC is shown in Fig. 3.

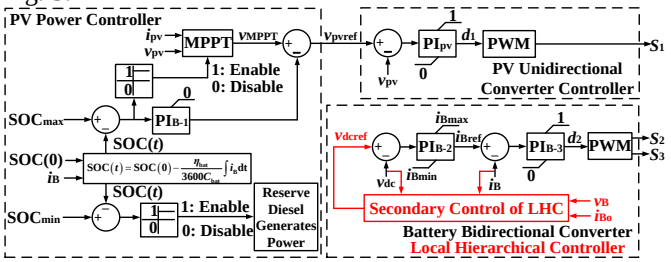

Fig. 3. Control block diagram of the proposed LHC for the PV-battery system in a standalone DC microgrid.

The primary control of the LHC is almost the same as the conventional battery control. The SOC of the battery packs are strictly regulated within the bounds. The stability of the PV-battery system controlled by the LHC are heuristically guaranteed by the bounds of the battery SOC and the bus voltage limits, according to the definition of power system stability in [46], which explains that the power system stability are accepted in the sense of boundaries. The only difference is that the bus voltage reference v_{dcref} is estimated by the secondary control of the LHC instead of a fixed nominal value. The secondary control of the LHC uses the measured values the DC bus voltage v_{dc}, output current of the battery system i_{Bo}, and the measured battery current i_{B} and battery voltage v_{B} from the BMS. Flowchart of the secondary control algorithm is depicted in Fig. 4.

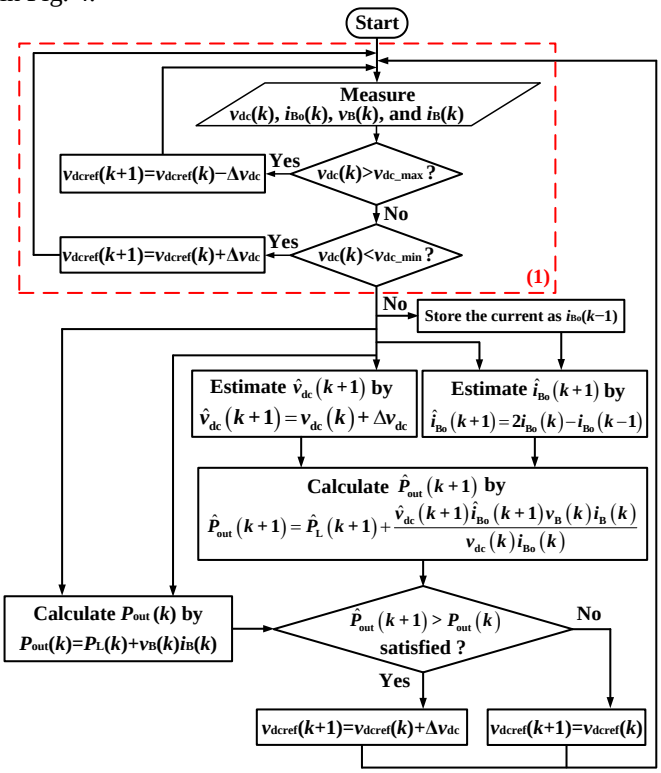

Fig. 4. Flowchart of the secondary control algorithm of the LHC.

Here, k indicates the sampling time kT_{s1} of the secondary control; T_{s1} is the sampling period; Δv_{dc} is the incremental bus voltage; $v_{\mathrm{dc\_max}}$ and $v_{\mathrm{dc\_min}}$ are the upper limit and the lower limit of the bus voltage; $\hat{v}_{\mathrm{dc}}$ and $\hat{\imath}_{\mathrm{Bo}}$ are the estimated bus voltage and the estimated output current of the battery system; $\hat{v}_{\mathrm{B}}$ and $\hat{\imath}_{\mathrm{B}}$ are the estimated voltage and the estimated current of the battery pack; and $\hat{P}_{\mathrm{out}}$ and $\hat{P}_{\mathrm{L}}$ are the estimated total output power and the estimated injected power into the DC microgrid. The process is specifically described as follows:

(1) v_{dc}, i_{Bo}, v_{B}, and i_{B} are measured at the sampling time kT_{s1} and v_{dc} is compared with the upper limit $v_{\mathrm{dc\_max}}$ and the lower limit $v_{\mathrm{dc\_min}}$. If $v_{\mathrm{dc}} > v_{\mathrm{dc\_max}}$, which means the DC bus voltage is greater than the upper limit, v_{dcref} reduces by the step of Δv_{dc} until v_{dc} is regulated within the tolerances. If $v_{\mathrm{dc}} < v_{\mathrm{dc\_min}}$, which means the DC bus voltage is less than the lower limit, v_{dcref} increases by the step of Δv_{dc} until v_{dc} is regulated within the tolerances.

(2) The measured v_{dc}, i_{Bo}, v_{B}, and i_{B} at the sampling time kT_{s1} and the stored i_{Bo} at the sampling time $(k\text{-}1)T_{s1}$ are used for the estimations of the total output power $\hat{P}_{\mathrm{out}}(k+1)$. First, v_{dc} at the sampling time $(k\text{+}1)T_{s1}$ is estimated using

$$\hat{v}_{\mathrm{dc}}(k+1) = v_{\mathrm{dc}}(k) + \Delta v_{\mathrm{dc}}. \tag{7}$$

According to the Kirchhoff's current law,

$$\frac{P_{\mathrm{pv}} - P_{\mathrm{loss\_pvc}}}{v_{\mathrm{dc}}} + i_{\mathrm{Bo}} = \frac{v_{\mathrm{dc}}}{R_{\mathrm{CRL}}} + \frac{P_{\mathrm{CRL}}}{v_{\mathrm{dc}}}, \tag{8}$$

where $P_{\mathrm{loss\_pvc}}$ is the power loss of the PV boost converter. Differentiating i_{Bo} by v_{dc} at the MPP gives

$$\frac{\partial i_{\mathrm{Bo}}}{\partial v_{\mathrm{dc}}} = \frac{1}{R_{\mathrm{CRL}}} - \frac{P_{\mathrm{CPL}} + P_{\mathrm{loss\_pvc}} - P_{\mathrm{pv}}}{v_{\mathrm{dc}}^2}. \tag{9}$$

Here, due to the incremental bus voltage Δv_{dc} is generally set less than 0.5% of the bus voltage v_{dc} (e.g. Δv_{dc}=0.24 V for v_{dcref}=48 V), the term $\frac{P_{\mathrm{CPL}}+P_{\mathrm{loss\_pvc}}-P_{\mathrm{pv}}}{v_{\mathrm{dc}}^2}$ can be considered as a constant during the two neighboring sampling times as

$$\begin{aligned} &\frac{P_{\mathrm{CPL}} + P_{\mathrm{loss\_pvc}} - P_{\mathrm{pv}}}{v_{\mathrm{dc}}^2} - \frac{P_{\mathrm{CPL}} + P_{\mathrm{loss\_pvc}} - P_{\mathrm{pv}}}{\left(v_{\mathrm{dc}} + \Delta v_{\mathrm{dc}}\right)^2} \\ &= \left(P_{\mathrm{CPL}} + P_{\mathrm{loss\_pvc}} - P_{\mathrm{pv}}\right) \frac{2\Delta v_{\mathrm{dc}} v_{\mathrm{dc}} + \Delta v_{\mathrm{dc}}^2}{v_{\mathrm{dc}}^2 \left(v_{\mathrm{dc}} + \Delta v_{\mathrm{dc}}\right)^2} \approx 0 \end{aligned}. \tag{10}$$

Then, i_{Bo} can be linearly estimated based on the measured i_{Bo} of the last two sampling times as

$$\hat{i}_{\mathrm{Bo}}(k+1) = i_{\mathrm{Bo}}(k) - \left[i_{\mathrm{Bo}}(k-1) - i_{\mathrm{Bo}}(k)\right]. \tag{11}$$

Reorganize (11), i_{Bo} at the sampling time $(k\text{+}1)T_{s1}$ is estimated using

$$\hat{i}_{\mathrm{Bo}}(k+1) = 2i_{\mathrm{Bo}}(k) - i_{\mathrm{Bo}}(k-1). \tag{12}$$

A graphic illustration is plotted in Fig. 5 to visualize the linear estimations of i_{Bo}.

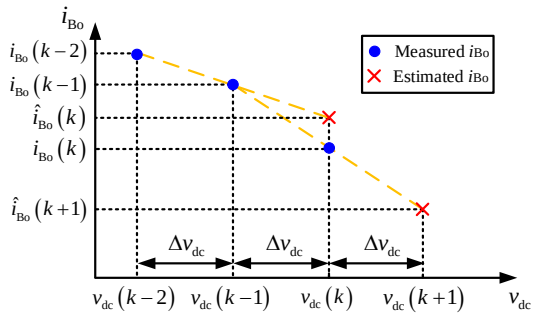

Fig. 5. Diagram of v_{dc} versus i_{Bo}.

Then, $\hat{P}_{\mathrm{out}}(k+1)$ is estimated based on $\hat{v}_{\mathrm{dc}}(k+1)$, $\hat{\imath}_{\mathrm{Bo}}(k+1)$, $v_{\mathrm{dc}}(k)$, $i_{\mathrm{Bo}}(k)$, $v_{\mathrm{B}}(k)$, and $i_{\mathrm{B}}(k)$ as

$$\hat{P}_{\text{out}}(k+1)=\hat{P}_{\text{L}}(k+1)+\frac{\hat{v}_{\text{dc}}(k+1)\hat{i}_{\text{Bo}}(k+1)v_{\text{B}}(k)i_{\text{B}}(k)}{v_{\text{dc}}(k)i_{\text{Bo}}(k)}. \quad (13)$$

Here, the power injected from the PV-battery system into the DC microgrid at the sampling time $(k+1)T_{s1}$ is $\hat{P}_{\text{L}}(k+1)$. Due to the loads in standalone DC microgrids can be generally modeled as an equivalent resistive load in parallel with an equivalent constant power load,

$$\hat{P}_{\text{L}}(k+1)=\frac{\hat{v}_{\text{dc}}^2(k+1)}{R_{\text{CRL}}}+P_{\text{CPL}}, \quad (14)$$

where the resistance of the equivalent resistive load R_{CRL} and the power of the equivalent constant power load P_{CPL} are required to be predetermined. Besides, the power of the battery pack at the sampling time $(k+1)T_{s1}$, $\hat{P}_{\text{Bi}}(k+1)$ can also be derived.

For the case of $v_{\text{dc}} > v_{\text{dcref}}$, the battery pack absorbs the excess power. Then, the efficiency of the battery bi-directional DC/DC converter at the sampling time kT_{s1} is

$$\eta_{\text{BC}}(k)=\frac{v_{\text{B}}(k)i_{\text{B}}(k)}{v_{\text{dc}}(k)i_{\text{Bi}}(k)}. \quad (15)$$

Besides, the efficiency of the battery bi-directional DC/DC converter can be considered as a constant during the two neighboring sampling times,

$$\hat{\eta}_{\text{BC}}(k+1)=\eta_{\text{BC}}(k). \quad (16)$$

Then, $\hat{P}_{\text{Bi}}(k+1)$ can be estimated as

$$\begin{aligned}\hat{P}_{\text{Bi}}(k+1)&=\hat{v}_{\text{dc}}(k+1)\hat{i}_{\text{Bo}}(k+1)\hat{\eta}_{\text{BC}}(k+1)\\&=\frac{\hat{v}_{\text{dc}}(k+1)\hat{i}_{\text{Bo}}(k+1)v_{\text{B}}(k)i_{\text{B}}(k)}{v_{\text{dc}}(k)i_{\text{Bo}}(k)}\end{aligned}. \quad (17)$$

For the case of $v_{\text{dc}} < v_{\text{dcref}}$, the battery pack provides the shortage power. Then, the efficiency of the battery bi-directional DC/DC converter at the sampling time kT_{s1} is

$$\eta_{\text{BC}}(k)=\frac{v_{\text{dc}}(k)i_{\text{Bo}}(k)}{v_{\text{B}}(k)i_{\text{B}}(k)} \quad (18)$$

and

$$\hat{\eta}_{\text{BC}}(k+1)=\frac{v_{\text{dc}}(k)i_{\text{Bo}}(k)}{v_{\text{B}}(k)i_{\text{B}}(k)}. \quad (19)$$

Then, $\hat{P}_{\text{Bi}}(k+1)$ can be estimated as

$$\begin{aligned}\hat{P}_{\text{Bi}}(k+1)&=\frac{\hat{v}_{\text{dc}}(k+1)\hat{i}_{\text{Bo}}(k+1)}{\hat{\eta}_{\text{BC}}(k+1)}\\&=\frac{\hat{v}_{\text{dc}}(k+1)\hat{i}_{\text{Bo}}(k+1)v_{\text{B}}(k)i_{\text{B}}(k)}{v_{\text{dc}}(k)i_{\text{Bo}}(k)}\end{aligned}. \quad (20)$$

Consider both (17) and (20), $\hat{P}_{\text{Bi}}(k+1)=\frac{\hat{v}_{\text{dc}}(k+1)\hat{i}_{\text{Bo}}(k+1)v_{\text{B}}(k)i_{\text{B}}(k)}{v_{\text{dc}}(k)i_{\text{Bo}}(k)}$ is a uniform expression for the battery power estimations.

(3) The total output power at the sampling time kT_{s1}, $P_{\text{out}}(k)$ is derived based on the measured $v_{\text{dc}}(k)$, $v_{\text{B}}(k)$, and $i_{\text{B}}(k)$ as

$$P_{\text{out}}(k)=\frac{v_{\text{dc}}^2(k)}{R_{\text{CRL}}}+P_{\text{CPL}}+v_{\text{B}}(k)i_{\text{B}}(k). \quad (21)$$

Then, $P_{\text{out}}(k)$ is compared with $\hat{P}_{\text{out}}(k+1)$ to determine $v_{\text{dcref}}(k+1)$. If $\hat{P}_{\text{out}}(k+1) > P_{\text{out}}(k)$, which means the output power can still be increased, $v_{\text{dcref}}(k+1)=v_{\text{dcref}}(k)+\Delta v_{\text{dc}}$. If $\hat{P}_{\text{out}}(k+1) \le P_{\text{out}}(k)$, which means the output power cannot be further increased, $v_{\text{dcref}}(k+1)=v_{\text{dcref}}(k)$. By tracking the references provided by the secondary control of the LHC, the primary control of the LHC can regulate the DC bus voltage to maximize the efficiency of the entire PV-battery system in real time. Importantly, the generation curtailment and the SOC control of the battery packs are still primary concerns in the extreme conditions. The proposed control strategy is designed based on these concerns.

III. Simulation Results

Simulations are carried out on MATLAB/SIMULINK with the solver type of Tustin at the sampling frequency of 200 kHz. The PV modules are BP Solar SX-3190B [47]. The specifications of the PV boost converters are listed in Table I. The MPPT control for the PV boost converters is the conventional P&O control [7]. The parameters of the PV power controller are listed in Table II. The battery packs are the Panasonic Valve Regulated Lead-Acid Battery LC-R127R2NA. The coefficient η_{bat} is set to be 1. The specifications of the battery bi-directional DC/DC converters are listed in Table III. The parameter values of the converters are selected based on the power quality and the dynamic performance of the PV-battery system. The parameters of the LHC are listed in Table IV. The nominal DC bus voltage is 48 V. The upper limit and the lower limit of the DC bus voltage are 50.4 V and 45.6 V, respectively. The sampling frequency of the MPPT control is 20 kHz. The sampling frequency of the conventional control and the LHC is 10 kHz.

TABLE I. Specifications of the PV Boost Converters

Parameter	Value
C_{pv}	300 μF
L_1	100.6 mH
ESR of L_1	11.6 mΩ
Forward voltage of the diode D_2, V_{fD2}	0.7 V
C_{cd1}	112 μF

TABLE II. Parameters of the PV Power Controller

Description	Value
Initial duty ratio of the P&O control	0.5
Duty ratio upper limit of the P&O control	0.9
Duty ratio lower limit of the P&O control	0.1
Incremental duty ratio of the P&O control	4×10^{-5}
Capacity of the battery pack, C_{bat}	36 Ah/20h
Initial SOC, SOC (0)	56%
Maximum SOC, SOC_{max}	90%
Minimum SOC, SOC_{min}	20%
Proportional of the $\text{PI}_{\text{B-1}}$	0.1
Integral of the $\text{PI}_{\text{B-1}}$	0.01
Proportional of the PI_{pv}	5
Integral of the PI_{pv}	30
Switching frequency	10 kHz

TABLE III. Specifications of the Battery Converters

Parameter	Value
C_{B}	112 μF
L_2	100.3 mH
ESR of L_2	11.8 mΩ
C_{cd2}	112 μF

TABLE IV. PARAMETERS OF THE LHC

Description	Value
Incremental bus voltage, Δv_{dc}	0.2 V
Upper limit of the bus voltage, v_{dc_max}	50.4 V
Lower limit of the bus voltage, v_{dc_min}	45.6 V
Resistance of the equivalent resistive load, R_{CRL}	26.03 Ω
Power of the constant power load, P_{CPL}	8.42 W
Proportional of the PI_{B-2}	1.5
Integral of the PI_{B-2}	50
Proportional of the PI_{B-3}	100
Integral of the PI_{B-3}	2
Switching frequency	20 kHz

A. Case Studies of One-PV-Module-Battery System

Case studies of a PV-battery system with one BP Solar SX-3190B module (1×1 module) are carried out using the irradiance profile at the Higher Polytechnic School of the Dakar University in Senegal on a sunny day in summer, as shown in Fig. 6. Fig. 7 and Fig. 8 show respectively the waveforms of the corresponding v_{dc} and P_{out} of the one-PV-module-battery system with the conventional control and that with the LHC. The SOC of the battery pack for both control schemes are plotted in Fig. 9. Apparently, both SOCs are within the bounds.

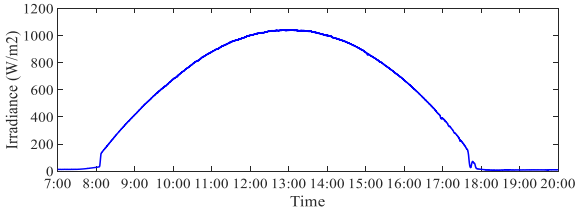

Fig. 6. An actual irradiance profile on a sunny day in simulation.

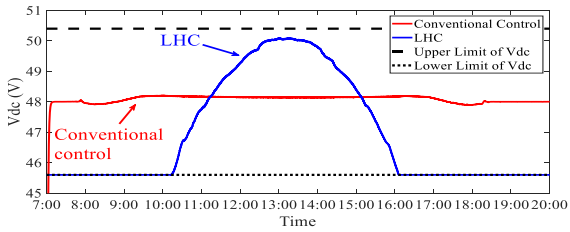

Fig. 7. Simulation waveforms of v_{dc} of the one-PV-module-battery system with the conventional control and the LHC on a sunny day.

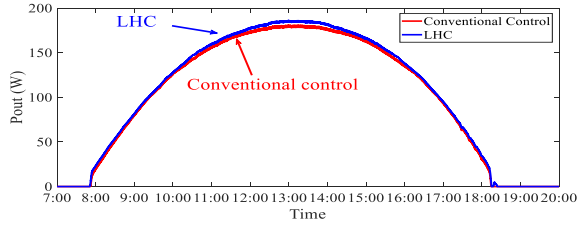

Fig. 8. Simulation waveforms of P_{out} of the one-PV-module-battery system with the conventional control and the LHC on a sunny day.

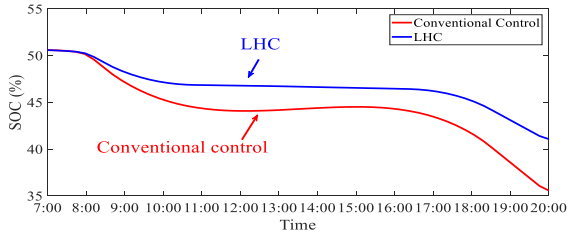

Fig. 9. SOC of the battery pack on a sunny day for both control schemes.

In Fig. 8, simulation waveforms of the corresponding P_{out} of the one-PV-module-battery system operating under an actual irradiance profile with both the conventional control and the LHC are presented. Obviously, more power can be harvested by the proposed LHC. Fig. 10 shows the cumulative extraction of E_{out} throughout the period of 13 hours for both controls. The results show that 3.3% more energy can be harvested by the proposed LHC. This signifies that the energy efficiency of the entire PV-battery system can be enhanced by 3.3% via the use of the LHC.

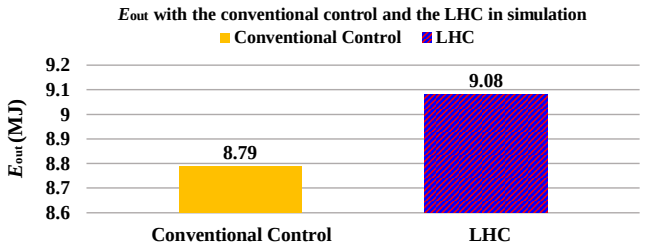

Fig. 10. Plots of E_{out} with the conventional control and the LHC using the actual irradiance profile in simulation.

Furthermore, the extreme conditions of SOC reaching SOC_{max} and SOC_{min} are investigated. When the initial SOC of the battery pack is 25% and the supplied power by the PV modules are insufficient, the battery pack discharges until the SOC reaches SOC_{min}, as shown in Fig. 11(a). When the initial SOC of the battery pack is 85% and the supplied power by the PV modules are redundant, the battery pack charges until the SOC reaches SOC_{max}, as shown in Fig. 11(b). Obviously, the SOC of the battery pack can be well regulated by the PV power controller within the bounds for the PV-battery system controlled by the conventional control and the proposed LHC.

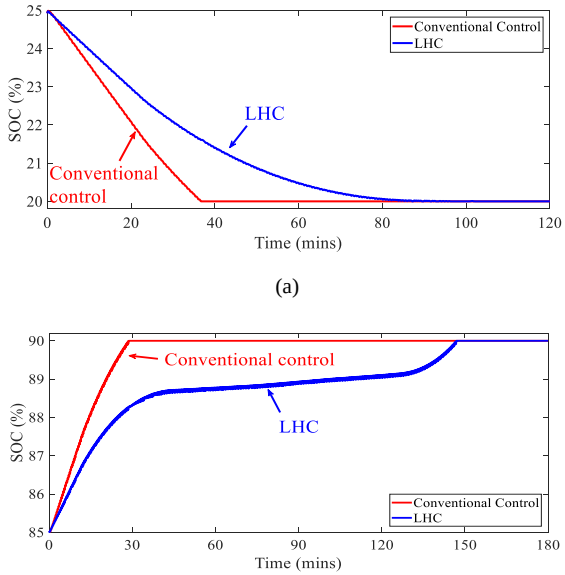

Fig. 11. SOC of the battery pack reaching (a) SOC_{min} and (b) SOC_{max} for both control schemes.

B. Case Studies of Multiple PV-Battery Systems

Case studies of 12 PV-battery systems with BP Solar SX-3190B modules are also carried out using the irradiance profile at Higher Polytechnic School of the Dakar University in Senegal on a cloudy day in summer, as shown in Fig. 12. Each

of the 12 PV modules contains 15 modules (3×5 modules). Three of the PV modules operate under the uniform insolation condition, while the other PV modules operate under partial shading conditions, as shown in Fig. 13. The waveforms of the total output power of the 12 PV-battery systems with both the conventional control and the LHC on the cloudy day are shown in Fig. 14. Compared with the PV-battery systems controlled by the conventional control, the PV-battery systems controlled by the LHC can inject more power into the DC microgrid. Fig. 15 shows the cumulative extraction of E_{out} for both control schemes. The results show that more energy about 4.7 kWh (2.84% more) can be harvested by using the LHC for the 12 PV-battery systems on the cloudy day.

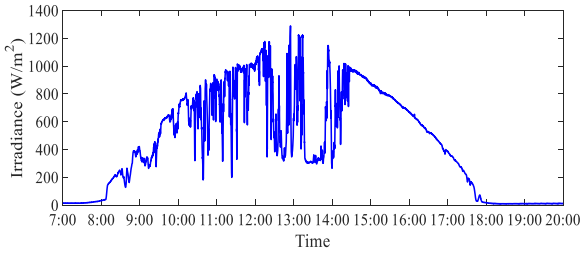

Fig. 12. An actual irradiance profile on a cloudy day in simulation.

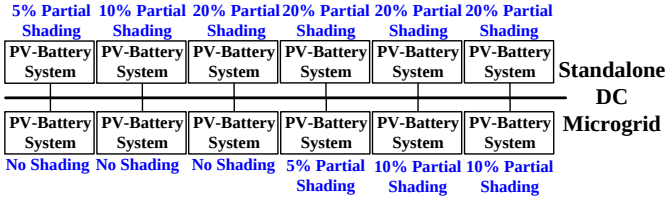

Fig. 13. Structure of the 12 PV-battery systems in a standalone DC microgrid.

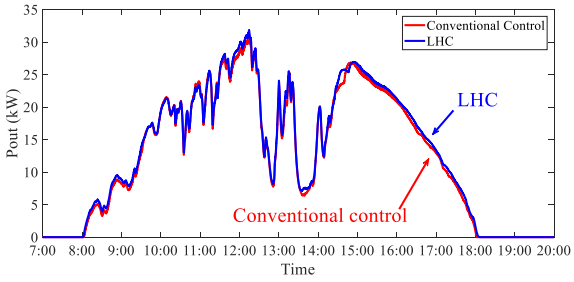

Fig. 14. Simulation waveforms of P_{out} of the 12 PV-battery systems with the conventional control and the LHC on a cloudy day.

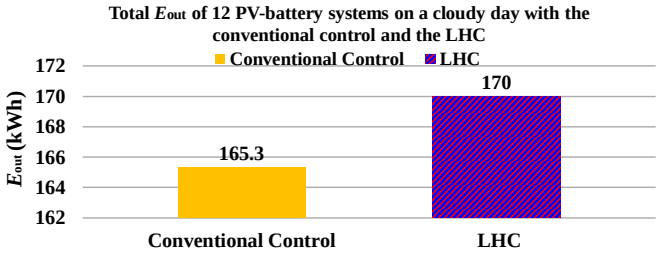

Fig. 15. Plots of E_{out} of the 12 PV-battery systems with the conventional control and the LHC on a cloudy day.

Case studies of a nominal 600-kW PV-battery system with BP Solar SX-3190B modules are also carried out using the sunny-day irradiance profile in Fig. 6. The waveforms of the total output power for both control schemes are shown in Fig. 16. The cumulative extraction of E_{out} for both control schemes are presented in Fig. 17. The results show that around 26.9 kWh more of energy can be harvested by the LHC for the 600-kW PV-battery system each day without any additional hardware costs. Assume the PV-battery systems controlled by the LHC are widely adopted in Senegal's solar home systems. According to the average electricity price in Senegal, which is 0.13 US dollars/kWh [48], the 600-kW PV-battery system can save more than 1200 US dollars per year. Considering the operating large solar PV plants in Senegal is about 2 MW (2016), more than four million US dollars can be saved per year by adopting the proposed LHC.

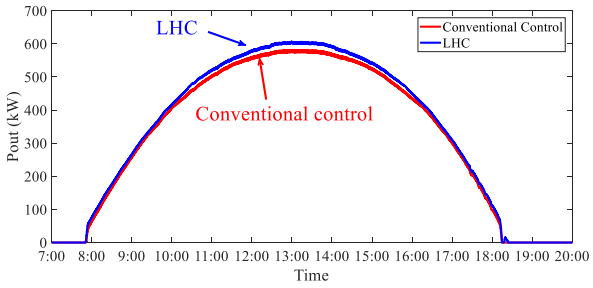

Fig. 16. Simulation waveforms of P_{out} of the 600-kW PV-battery system with the conventional control and the LHC on a sunny day.

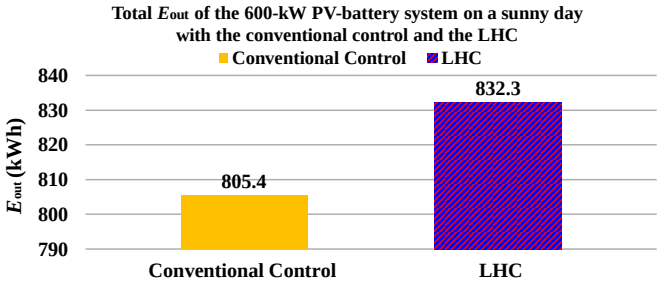

Fig. 17. Plots of E_{out} of the 600-kW PV-battery system with the conventional control and the LHC on a sunny day.

IV. Experimental Verification

Experiments are carried out on a one-PV-module-battery system. The PV module of BP Solar SX-3190B is emulated using the TerraSAS™ series Photovoltaic Simulator. Some values of the irradiances and the corresponding MPP of P_{pv}, v_{pv}, and i_{pv} are listed in Table V. The standalone DC microgrid is emulated using resistive loads and the Ametek E-load PLA5K-800-100E. Specifications of the PV boost converter, the battery bi-directional DC/DC converter, and the battery pack are identical with the specifications in simulation. The part numbers and prices of the components used for the converters are listed in Table VI. All the selected components are cost efficient. The sampling frequency of the MPPT control is 20 kHz. The sampling frequency of the conventional control and the LHC is 10 kHz. The coefficient η_{bat} is estimated to be 0.96 based on the offline measurements of the open-circuit voltage and ambient temperature of the battery pack.

TABLE V. Irradiance and the Corresponding MPP of P_{PV}, v_{PV}, i_{PV}

Irradiance (W/m²)	P_{PV} (W)	v_{PV} (V)	i_{PV} (A)
920	172.4	24.1	7.2
500	92.1	23.6	3.9
750	140.8	23.9	5.9
1000	187.6	24.3	7.8

TABLE VI. LIST OF COMPONENTS USED FOR THE CONVERTERS

Component	Part No.	Est. cost per unit (in US dollars)
C_{pv}	EGPD101ELL301MK30H	0.35
C_B, C_{d1}, C_{d2}	EGXF161ELL111	0.1
L_1, L_2, L_3	Custom-made	0.35
D_1, D_2	PMEG6020	0.03
MOSFETs	SQD50N10-8M9L_GE3	0.3
Gate driver	VO3150A-X007T	0.25
Sensing resistor	14AFR047E	0.28
Op-amp	LM324	0.05
Comparator	TS391	0.06

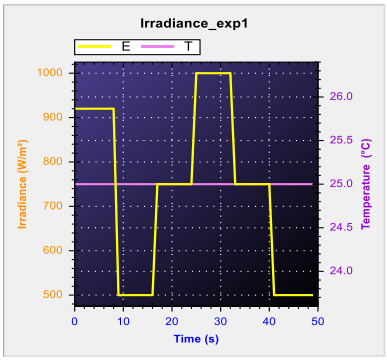

Fig. 18. Irradiance profile for the PV module in experiment.

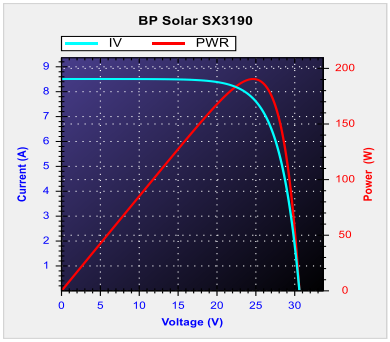

Fig. 19. Characteristic curves of the modeled PV module in experiment.

Initially, the irradiance of the PV module without the battery system is set to vary from 920 W/m^2 to 500 W/m^2 to 750 W/m^2 to 1000 W/m^2 to 750 W/m^2 and to 500 W/m^2, as shown in Fig. 18. Fig. 19 shows the characteristic curves of the modeled PV module used in experiment, which are identical to the curves obtained in simulation and given in the datasheet. The corresponding v_{pv}, i_{pv}, and P_{pv}, are shown in Fig. 20. Apparently, v_{pv}, i_{pv}, and P_{pv} at steady state are well-regulated to track the MPP for different irradiances. The corresponding v_{dc} are shown in Fig. 21. v_{dc} at steady state varies with offsets when the irradiance changes. Clearly, the steady-state v_{dc} during the intervals of 35.1 V, 41.8 V, and 51.1 V are out of the limits of the bus voltage (45.6 V~50.4 V). This violates the voltage requirement of the standalone DC microgrid.

Next, the battery system is incorporated with the conventional control. The waveforms of v_{pv}, i_{pv}, and P_{pv} are shown in Fig. 22. Apparently, v_{pv}, i_{pv}, and P_{pv} at steady state are also well-regulated to track the MPP for different irradiances. In Fig. 23, the bus voltages at steady state are well-regulated at the nominal values for different irradiances. Therefore, the effectiveness of the battery system in stabilizing the DC bus voltage is hereby experimentally illustrated. Besides, the waveforms of P_L and P_{Bi} are shown in Fig. 23 and Fig. 24, respectively. Then, P_{out} at steady state can be calculated based on the measured values of P_L and P_{Bi}, which are 122.2 W, 84.7 W, 102.7 W, 129.8 W, 102.7 W, and 84.7 W, respectively for various irradiance levels.

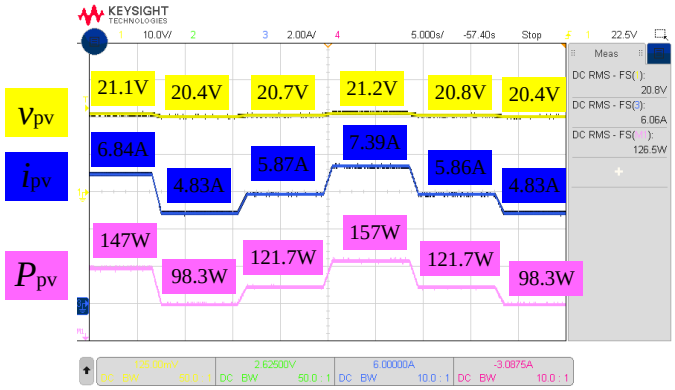

Fig. 20. Waveforms of v_{pv}, i_{pv}, and P_{pv} without the battery system in experiment.

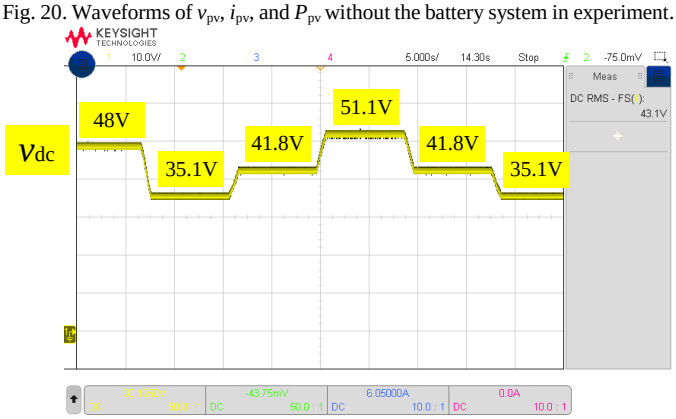

Fig. 21. Waveforms of v_{dc} without the battery system in experiment.

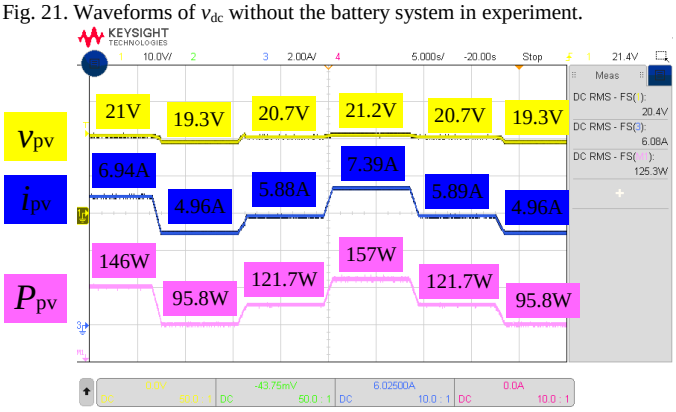

Fig. 22. Waveforms of v_{pv}, i_{pv}, and P_{pv} with the battery system controlled by the conventional control.

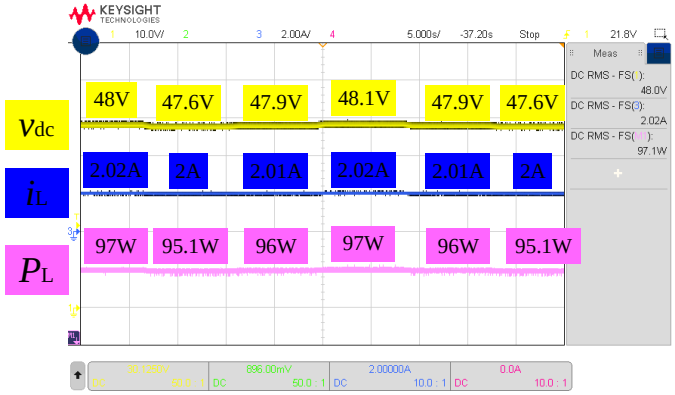

Fig. 23. Waveforms of v_{dc}, i_L, and P_L with the battery system controlled by the conventional control.

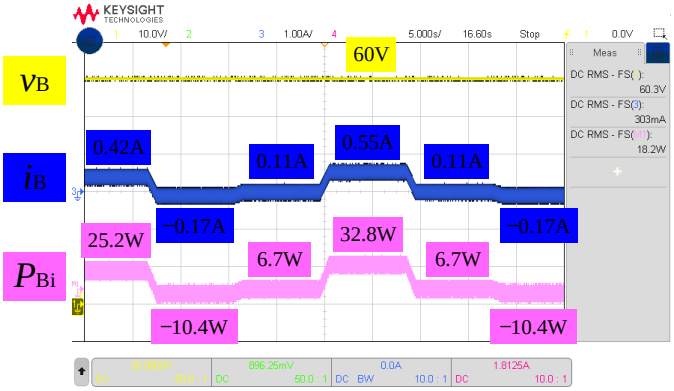

Fig. 24. Waveforms of v_B, i_B, and P_{Bi} with the battery system controlled by the conventional control.

Then, the one-PV-module-battery system is controlled by the proposed LHC. Waveforms of the measured v_{pv}, i_{pv}, and P_{pv} are shown in Fig. 25. Again, v_{pv}, i_{pv}, and P_{pv} at steady state are well-regulated to MPP for different irradiances. In Fig. 26, it is shown that v_{dc} of the standalone DC microgrid is well-regulated within the limits of the bus voltage (45.6 V~50.4 V). P_L and P_{Bi} are shown in Fig. 26 and Fig. 27, respectively. Then, P_{out} at steady state can be calculated based on the measured values of P_L and P_{Bi}, which are 125.3 W, 87.2 W, 104.3 W, 133.5 W, 104.3 W, and 87.2 W, respectively for the various irradiance levels. Compared with the P_{out} of the one-PV-module-battery system controlled by the conventional control, the efficiency improvement at the respective irradiance level are about 3.24%, 2.95%, 1.55%, 2.84%, 1.55%, and 2.95%, as shown in Fig. 28.

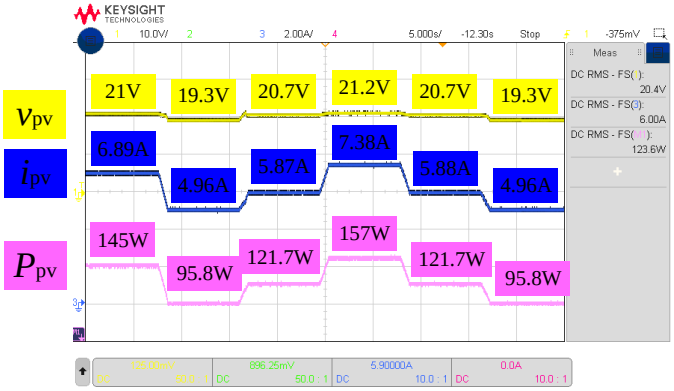

Fig. 25. Waveforms of v_{pv}, i_{pv}, and P_{pv} with the battery system controlled by the LHC.

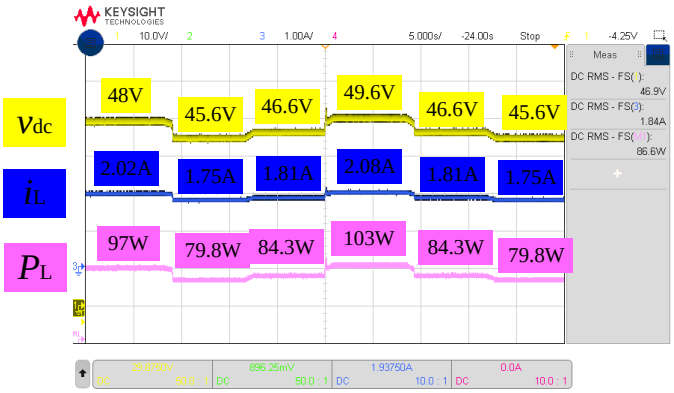

Fig. 26. Waveforms of v_{dc}, i_L, and P_L with the battery system controlled by the LHC.

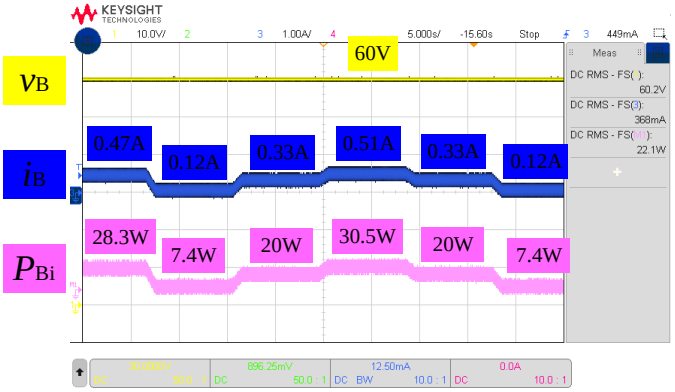

Fig. 27. Waveforms of v_B, i_B, and P_{Bi} with the battery system controlled by the LHC.

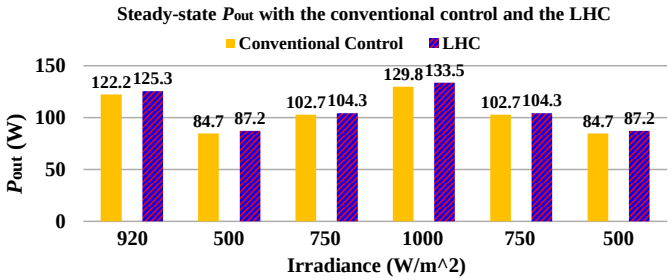

Fig. 28. Plots of the steady-state P_{out} of the one-PV-module-battery system controlled by the conventional control and the LHC.

For practical sake but without the loss of accuracy, the time scale of the irradiance profile of the sunny day in Fig. 6 is shortened to one hundred seconds (around 13:00) in the experiment, as shown in Fig. 29. Based on the measured P_L and P_{Bi}, P_{out} of the one-PV-module-battery system with both control methods can be plotted, as shown in Fig. 30. By integrating P_{out}, the cumulative extraction of E_{out} throughout the one-hundred-second period for both control methods can be obtained and plotted as shown in Fig. 31. From the results, it is found that there is 3.2% efficiency improvement via the use of the LHC.

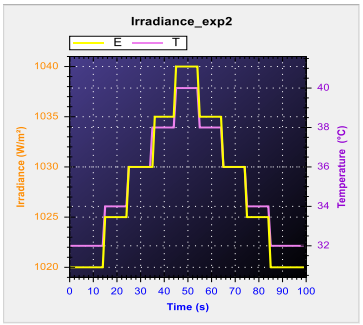

Fig. 29. Irradiance profile of a shortened sunny day in experiment.

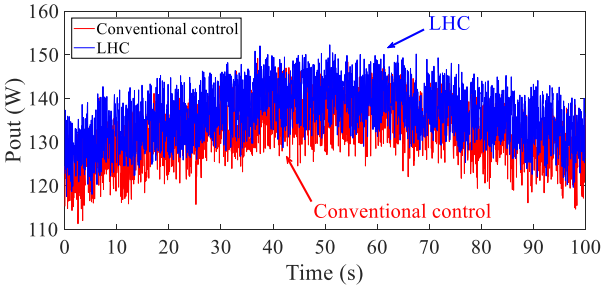

Fig. 30. Waveforms of P_{out} with the conventional control and the LHC using the irradiance profile on a shortened sunny day in experiment.

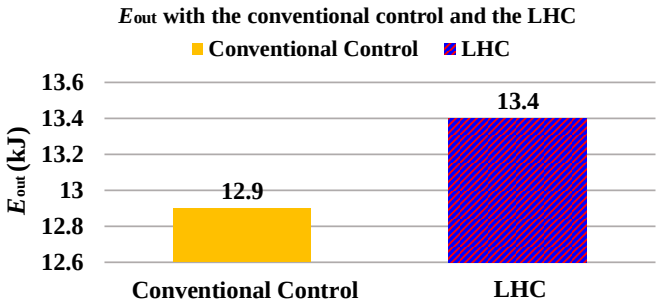

Fig. 31. Plots of E_{out} with the conventional control and the LHC using the irradiance profile on a shortened sunny day in experiment.

Experiments are also carried out on the one-PV-module-battery system emulating BP Solar SX-3190B, SunPower SPR-305-WHT, and SunTech STP270-24-Vb using the shortened irradiance profile within one hundred seconds (around 13:00) of the sunny day in Fig. 6 and the cloudy day in Fig. 12. The waveforms of the measured P_{out} for both control methods are plotted in Fig. 32. Obviously, the proposed LHC can always harvest more energy than the conventional control for different types of PV modules. The comparisons of E_{out} throughout one-hundred-second periods for different PV modules between two control methods are presented in Fig. 33. From the results, more than 3% efficiency improvement can be achieved for all the cases by adopting the LHC, i.e., 5.45% for BP Solar SX-3190B on the cloudy day, 4.5% for SunPower SPR-305-WHT on the sunny day, 4.81% for SunPower SPR-305-WHT on the cloudy day, 3.47% for SunTech STP270-24-Vb on the sunny day, 3.75% for SunTech STP270-24-Vb on the cloudy day.

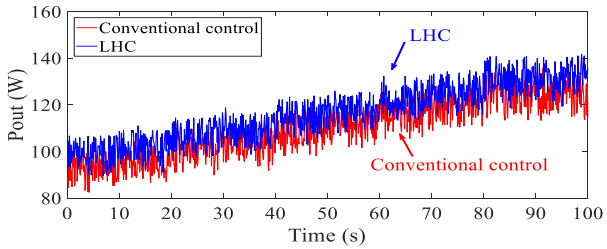

(a) BP Solar SX-3190B, cloudy day

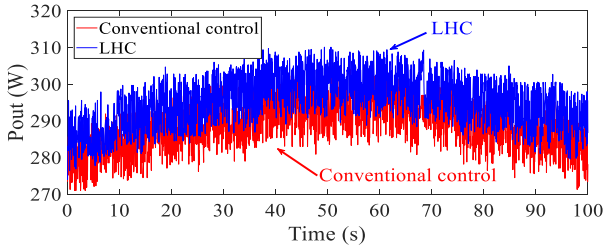

(b) SunPower SPR-305-WHT, sunny day

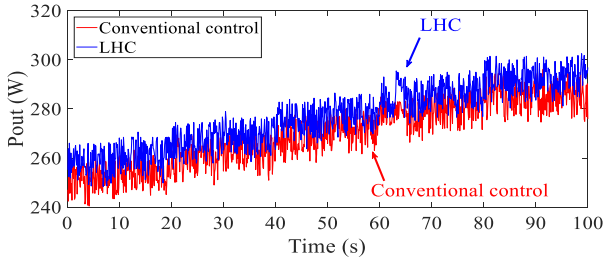

(c) SunPower SPR-305-WHT, cloudy day

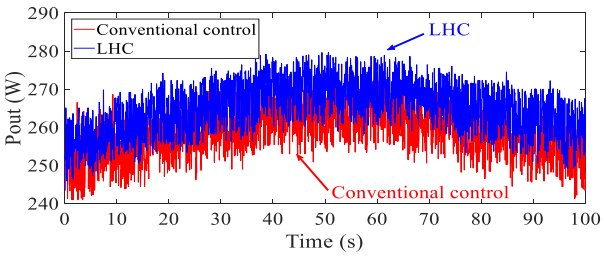

(d) SunTech STP270-24-Vb, sunny day

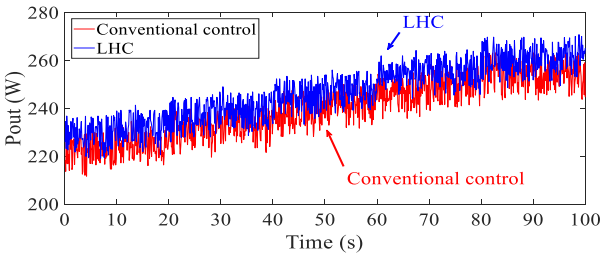

(e) SunTech STP270-24-Vb, cloudy day

Fig. 32. Waveforms of P_{out} for different PV modules using the irradiance profile on a shortened sunny and cloudy day in experiment.

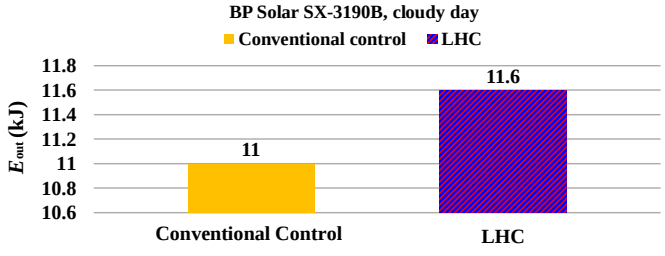

(a)

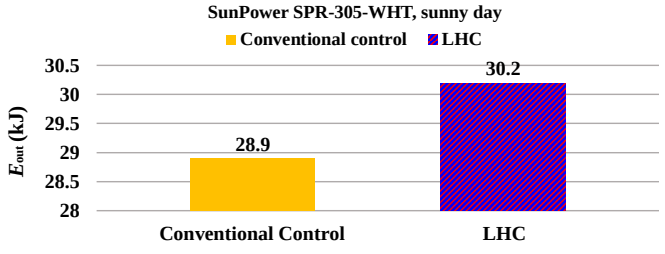

(b)

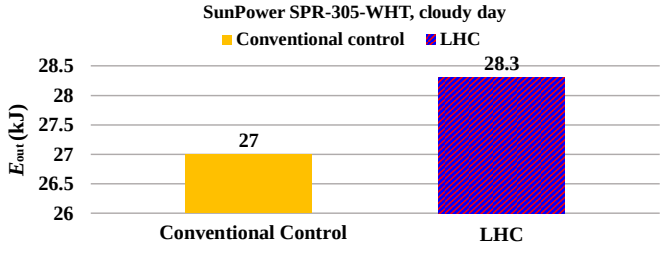

(c)

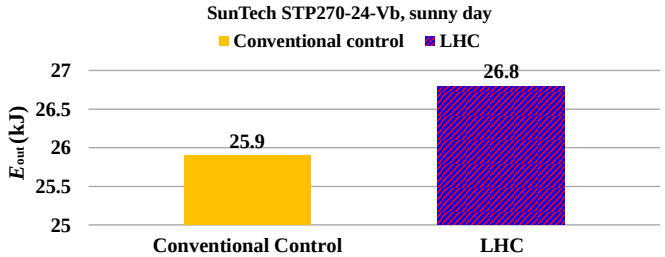

(d)

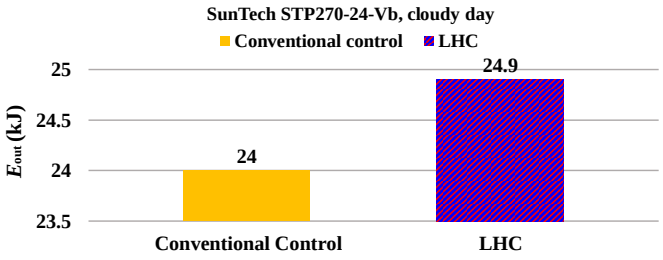

(e)

Fig. 33. Plots of E_{out} for different PV modules using the irradiance profile on a shortened sunny and cloudy day in experiment.

V. Conclusions

In this paper, a local hierarchical control (LHC) is proposed for the battery system to improve the efficiency of the entire PV-battery system in a standalone DC microgrid without additional hardware costs. The secondary control of the LHC estimates the optimal references for the primary control of the LHC to manage the power flow of the entire PV-battery system. Both simulation and experimental results validate the efficiency improvement of the one-PV-module-battery systems controlled by the LHC, which is about 3.3% for the actual irradiance profile in a sunny day in simulation and more than 3% for the one-hundred-second irradiance profiles on both sunny and cloudy days using different types of PV modules and cost-efficient components for the converters in experiment. Additionally, case studies of multiple PV-battery systems show that 2.84% more energy can be harvested for a 12-PV-battery system under either the uniform/nonuniform insolation conditions on a cloudy day and more than 1200 US dollars can be saved (26.9 kWh more energy can be harvested) for a 600-kW PV-battery system on a sunny day in Senegal by adopting the LHC.

Acknowledgement

This work was supported by the theme-based research project T23-701/14-N.

References

[1] H. Häberlin, *Photovoltaics System Design and Practice*, Hoboken: Wiley, 2012.

[2] International renewable energy agency. *Solar PV in Africa: Costs and markets* [Online]. Available: https://www.irena.org/DocumentDownloads//Publications/IRENA_Solar_PV_Costs_Africa_2016.pdf.

[3] Y. M. Chen, A. Q. Huang, and X. Yu, "A high step-up three-port DC-DC converter for standalone PV/battery power systems," *IEEE Trans. Power Electron.*, vol. 28, no. 11, pp. 5049−5062, Nov. 2013.

[4] F. Nejabatkhah, S. Danyali, S. H. Hosseini, M. Sabahi, and S. M. Niapour, "Modeling and control of a new three-input DC-DC boost converter for hybrid PV/FC/battery power system," *IEEE Trans. Power Electron.*, vol. 23, no. 2, pp. 782−792, Mar. 2008.

[5] T. Cheng, D. C. Lu, and L. Qin, "Non-isolated single-inductor DC/DC converter with fully reconfigurable structure for renewable energy applications," *IEEE Trans. Circuit Syst. II, Exp. Briefs*, vol. 4, no. 3, pp. 1558−1566, Sep. 2013.

[6] A. Kwasinski, "Quantitative evaluation of DC microgrids availability: effects of system architecture and converter topology design choices," *IEEE Trans. Power Electron.*, vol. 26, no. 3, pp. 835−851, Dec. 2010.

[7] Y. Yang, K. A. Kim, F. Blaabjerg, and A. Sangwongwanich, *Advances in Grid-Connected Photovoltaic Power Conversion Systems*, Publisher: Woodhead Publishing, 2018.

[8] A. M. Dizqah, A. Maheri, K. Busawon, and P. Fritzson, "Standalone DC microgrids as complementarity dynamical systems: modeling and applications," *Control Eng. Practice*, vol. 35, pp. 102−112, Feb. 2015.

[9] A. P. N. Tahim, D. J. Pagano, and E. Ponce, "Nonlinear control of dc-dc bidirectional converters in standalone dc microgrids," in *Annu. Conf. Decision Control (CDC)*, 2013, pp. 3068−3073.

[10] J. T. C. Neto, A. O. Salazar, and A. L. Maitelli, "One cycle control applied to a standalone photovoltaic system for DC microgrid applications," in *Annu. Conf. Ind. Electron. Soc.*, 2016, pp. 3074−3079.

[11] E. Koutroulis and F. Blaabjerg, "Overview of maximum power point tracking techniques for photovoltaic energy production systems," *Elect. Power Components Syst.*, vol. 43, no. 12, pp. 1329−1351, Jul. 2015.

[12] A. Tah and D. Das, "An enhanced droop control method for accurate load sharing and voltage improvement of isolated and interconnected DC microgrids," *IEEE Trans. Sustain. Energy*, vol. 7, no. 3, pp. 1194−1204, Jul. 2016.

[13] A. M. Dizqah, A. Maheri, K. Busawon, and A. Kamjoo, "A multivariable optimal energy management strategy for standalone DC microgrids," *IEEE Trans. Power Syst.*, vol. 30, no. 5, pp. 2278−2287, Sept. 2015.

[14] X. Lu, J. M. Guerrero, K. Sun, and J. C. Vasquez, "An improved droop control method for DC microgrids based on low bandwidth communication with DC bus voltage restoration and enhanced current sharing accuracy," *IEEE Trans. Power Electron.*, vol. 29, no. 4, pp. 1800−1812, Apr. 2014.

[15] C. Li, F. Bosio, F. Chen et. al., "Economic dispatch for operating cost minimization under real-time pricing in droop-controlled DC microgrid," *IEEE J. Sel. Topics Power Electron.*, vol. 5, no. 1, pp. 587−595, Mar. 2017.

[16] W. R. Issa, M. A. Abusara, and S. M. Sharkh, "Control of transient power during unintentional islanding of microgrids," *IEEE Trans. Power Electron.*, vol. 30, no. 8, pp. 4573−4584, Aug. 2015.

[17] A. Sangwongwanich, Y. Yang, and F. Blaabjerg, "High-performance constant power generation in grid-connected PV systems" *IEEE Trans. Power Electron.*, vol. 31, no. 3, pp. 1822−1825, Mar. 2016.

[18] M. Rodriguez, G. Stahl, L. Corradini, and D. Maksimovic, "Smart DC power management system based on software-configurable power modules," *IEEE Trans. Power Electron.*, vol. 28, no. 4, pp. 1571−1586, Apr. 2013.

[19] A. Sangwongwanich, Y. Yang, F. Blaabjerg, and D. Sera, "Delta power control strategy for multistring grid-connected PV inverters" *IEEE Trans. Industry Appl.*, vol. 53, no. 3, pp. 3862−3870, Jul. 2017.

[20] Z. Zhang, Y. Y. Cai, Y. Zhang, D. J. Gu, and Y. F. Liu, "A distributed architecture based on microbank modules with self-reconfiguration control to improve the energy efficiency in the battery energy storage system," *IEEE Tran. Power Electron.*, vol. 31, no. 1, pp. 304−317, Jan. 2016.

[21] S. Peyghami, H. Mokhtari, P. Davari, P. C. Loh, and F. Blaabjerg, "On secondary control approaches for voltage regulation in DC microgrids," *IEEE Tran. Ind. Appl.*, vol. 53, no. 5, pp. 4855−4862, Sept. 2017.

[22] L. Che and M. Shahidehpour, "DC microgrids: economic operation and enhancement of resilience by hierarchical control," *IEEE Tran. Smart Grid*, vol. 5, no. 5, pp. 2517−2526, Sept. 2014.

[23] J. Umuhoza, Y. Zhang, S. Zhao, and A. Mantooth, "An adaptive control strategy for power balance and the intermittency mitigation in battery-PV energy system at residential DC microgrid level," in *Applied Power Electron. Confer. and Expo. (APEC)*, 2017, pp. 1341−1345.

[24] J. Ma, L. Yuan, Z. Zhao, and F. He, "Transmission loss optimization-based optimal power flow router strategy by hierarchical control for DC microgrids," *IEEE Tran. Power Electron.*, vol. 32, no. 3, pp. 1952−1963, Mar. 2017.

[25] Y. Yang, K. T. Mok, S. C. Tan, and S. Y. R. Hui, "Nonlinear dynamic power tracking of low-power wind energy conversion system," *IEEE Tran. Power Electron.*, vol. 30, no. 9, pp. 5223−5236, Sept. 2015.

[26] Y. Yang, S. C. Tan, and S. Y. R. Hui, "Mitigating distribution power loss of DC microgrids with DC electric springs," *IEEE Trans. Smart Grid*, vol. 9, no. 6, Nov. 2018.

[27] A. Kwasinski and C. N. Onwuchekwa, "Dynamic behavior and stabilization of dc microgrids with instantaneous constant-power loads," *IEEE Tran. Power Electron.*, vol. 26, no. 3, pp. 822−834, Mar. 2011.

[28] N. Bottrell, M. Prodanovic, and T. C. Green, "Dynamic stability of a microgrid with an active load," *IEEE Tran. Power Electron.*, vol. 28, no.11, pp. 5107−5119, Nov. 2013.

[29] T. L. Vandoorn, B. Meersman, L. Degroote, et. al., "A control strategy for islanded microgrids with DC-link voltage control," *IEEE Tran. Power Del.*, vol. 26, no. 2, pp. 703−713, Apr. 2011.

[30] S. Anand and B. G. Fernandes, "Reduced-order model and stability analysis of low-voltage DC microgrid," *IEEE Tran. Ind. Electron*, vol. 60, no.11, pp. 5040−5049, Nov. 2013.
[31] D. Chen, L. Xu, and L. Yao, "DC voltage variation based autonomous control of DC microgrids," *IEEE Tran. Power Del.*, vol. 28, no. 2, pp. 637−648, Apr. 2013.
[32] Y. Gu, W. Li, and X. He, "Frequency-coordinating virtual impedance for autonomous power management of DC microgrid," *IEEE Tran. Power Electron.*, vol. 30, no. 4, pp. 2328−2337, Apr. 2015.
[33] R. S. Balog, W. W. Weaver, and P. T. Krein, "The loads as an energy asset in a distributed DC smartgrid architecture," *IEEE Tran. Smart Grid*, vol. 3, no. 1, pp. 253−260, Mar. 2012.
[34] A. P. N. Tahim, D. J. Pagano, E. Lenz, and V. Stramosk, "Modeling and stability analysis of islanded DC microgrids under droop control," *IEEE Tran. Power Electron.*, vol. 30, no. 8, pp. 4597−4607, Aug. 2015.
[35] S. R. Huddy and J. D. Skufca, "Amplitude death solutions for stabilization of DC microgrids with instantaneous constant-power loads," *IEEE Tran. Power Electron.*, vol. 28, no. 1, pp. 247−253, Jan. 2013.
[36] M. Garcia, J. M. Maruri, L. Marroyo, E. Lorenzo, and M. Perez, "Partial shadowing, MPPT performance and inverter configurations: observations at tracking PV plants," *Progress in Photovoltaics: Research and Applications*, vol. 16, no. 6, pp. 529−536, Apr. 2008.
[37] L. Maharjan, S. Inoue, H. Akagi, and J. Asakura, "State-of-charge (SOC)-balancing control of a battery energy storage system based on a cascade PWM converter," *IEEE Trans. Power Electron.*, vol. 24, no. 6, pp. 1628−1636, Jun. 2009.
[38] M. Coleman, C. K. Lee, C. Zhu, and W. G. Hurley, "State-of-charge determination from EMF voltage estimation: using impedance, terminal voltage, and current for lead-acid and lithium-ion batteries," *IEEE Trans. Ind. Electron.*, vol. 54, no. 5, pp. 2550−2557, Oct. 2007.
[39] Y. Li and Y. Han, "A new perspective on battery cell balancing: thermal balancing and relative temperature control," in *Energy Conver. Congr. Expo. (ECCE)*, 2016, pp. 1−6.
[40] Y. Shang, B. Xia, N. Cui, C. Zhang, and C. Mi, "An automotive on-board ac heater without external power supplies for lithium-ion batteries at low temperatures," *IEEE Trans. Power Electron.*, vol. 33, no. 9, pp. 7759−7769, Sept. 2018.
[41] K. Jin, X. Ruan, M. Yang, and M. Xu, "A hybrid fuel cell power system," *IEEE Trans. Ind. Electron.*, vol. 56, no. 4, pp. 1212−1222, Apr. 2009.
[42] Z. Jiang and R. A. Dougal, "A compact digitally controlled fuel cell/battery hybrid power source," *IEEE Trans. Ind. Electron.*, vol. 53, no. 4, pp. 1094−1104, Aug. 2006.
[43] A. Khaligh, A. M. Rahimi, Y. Lee, and J. Chao, et. al., "Digital control of an isolated active hybrid fuel cell/li-ion battery power supply," *IEEE Trans. Veh. Technol.*, vol. 56, no. 6, pp. 3709−3721, Nov. 2007.
[44] M. Wang, C. K. Lee, S. C. Tan, and S. Y. R. Hui, "A configuration of storage system for DC microgrids," *IEEE Trans. on Power Electron.*, vol. 33, no. 5, pp. 3722–3733, May 2018
[45] S. Armstrong, M. E. Glavin, and W. G. Hurley, "Comparison of battery charging algorithms for standalone photovoltaic systems," in *IEEE Power Electron. Special. Conf.*, 2008, pp. 1469−1475.
[46] P. Kundur, J. Paserba, V. Ajjarapu, et. al., "Definition and classification of power system stability," *IEEE Trans. Power Syst.*, vol. 19, no. 3, pp. 1387−1401, Aug. 2004.
[47] "SX 3190B," GreenTech Solar USA, 2009, *http://www.greentechsolarusa.com/products/bpsolar/BP_190W.pdf*.
[48] International renewable energy agency. *Solar PV in Africa: Costs and markets* [Online]. Available: https://www.irena.org/publications/2016/Sep/Solar-PV-in-Africa-Costs-and-Markets.

Yun Yang (S'13–M'18) received the B.S. degree in electrical engineering from Wuhan University, Wuhan, China, in 2012 and Ph.D. degree in power electronics from Department of Electrical and Electronic Engineering, The University of Hong Kong, Hong Kong, in 2017. He is currently a Postdoctoral Research Fellow in the Department of Electrical and Electronic Engineering, The University of Hong Kong. He has published more than 20 technical papers. He won the outstanding presentation award in APEC 2016 and served as a session chair in IEEE PELS Workshop on Emerging Technologies: Wireless Power 2018. His current research interests include power electronics and control, microgrids, and wireless power transfer.

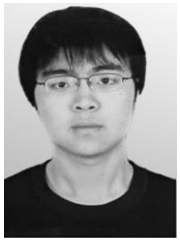

Yaxiao Qin received the B.S. degree in electrical engineering from Shandong University, Jinan, China. He received the M.Sc degree at the Department of Electrical and Computer Engineering, from Virginia Polytechnic Institute and State University, Blacksburg, U.S. He is currently pursuing his Ph.D degree in electrical and electronic engineering from The University of Hong Kong, Hong Kong. He has authored or coauthored more than 10 technical papers. He received the first prize paper award of IEEE Transactions on Power Electronics in 2009. His current research interests include high efficiency power converters, LED driving circuits, power electronics techniques in micro-grid, and low voltage high-current conversion techniques.

Siew-Chong Tan (S'00–M'06–SM'11) received the B.Eng. (Hons.) and M.Eng. degrees in electrical and computer engineering from the National University of Singapore, Singapore, in 2000 and 2002, respectively, and the Ph.D. degree in electronic and information engineering from the Hong Kong Polytechnic University, Hong Kong, in 2005. He is currently a Professor in Department of Electrical and Electronic Engineering, The University of Hong Kong, Hong Kong. Prof. Tan is an Associate Editor of the IEEE Transactions on Power Electronics. His research interests are focused in the areas of power electronics and control, smart grids, and clean energy technologies.

Ron Hui (M'87–SM'94–F'03) received his BSc (Eng) Hons at the University of Birmingham in 1984 and a D.I.C. and PhD at Imperial College London in 1987. Presently, he holds the Philip Wong Wilson Wong Chair Professorship at the University of Hong Kong and a Chair Professorship at Imperial College London. He has published over 300 technical papers, including more than 220 refereed journal publications. Over 60 of his patents have been adopted by industry. He is an Associate Editor of the IEEE Transactions on Power Electronics and IEEE Transactions on Industrial Electronics, and an Editor of the IEEE Journal of Emerging and Selected Topics in Power Electronics. His inventions on wireless charging platform technology underpin key dimensions of Qi, the world's first wireless power standard, with freedom of positioning and localized charging features for wireless charging of consumer electronics. He received the IEEE Rudolf Chope R&D Award from the IEEE Industrial Electronics Society and the IET Achievement Medal (The Crompton Medal) in 2010, and IEEE William E. Newell Power Electronics Award in 2015. He is a Fellow of the Australian Academy of Technological Sciences & Engineering (since 2010), the Royal Academy of Engineering, U.K (since 2016), and US Academy of Inventors (since 2018).